Published by IOP Publishing for Sissa Medialab

Received: *September 29, 2023*
Accepted: *December 4, 2023*
Published: *January 17, 2024*

24th International Workshop on Radiation Imaging Detectors
Oslo, Norway
25–29 June 2023

Advances in the TCAD modelling of non-irradiated and irradiated Low-Gain Avalanche Diode sensors

T. Croci,[a,*] **A. Morozzi,**[a] **A. Fondacci,**[c] **L. Lanteri,**[e] **F. Siviero,**[e] **V. Sola,**[e,d] **M. Ferrero,**[d] **L. Menzio,**[e] **R. Mulargia,**[e] **R. Arcidiacono,**[f,d] **N. Cartiglia,**[d] **G.M. Bilei,**[a] **D. Passeri**[c,a] **and F. Moscatelli**[b,a]

[a] *INFN, Perugia Unit, via A. Pascoli 23c, 06123 Perugia, Italy*
[b] *CNR-IOM, Perugia Unit, via A. Pascoli 23c, 06123 Perugia, Italy*
[c] *Engineering Department, University of Perugia, via G. Duranti 93, 06125 Perugia, Italy*
[d] *INFN, Torino Unit, via P. Giuria 1, 10125 Torino, Italy*
[e] *Physics Department, University of Torino, via P. Giuria 1, 10125 Torino, Italy*
[f] *Università del Piemonte Orientale, Largo Donegani 2/3, 20100 Novara, Italy*

E-mail: tommaso.croci@pg.infn.it

Abstract: The recently developed Low-Gain Avalanche Diode (LGAD) technology has gained growing interest within the high-energy physics (HEP) community, thanks to its capability of internal signal amplification that improves the particle detection. Since the next generation of HEP experiments will require tracking detectors able to efficiently operate in environments where expected fluences will exceed 1×10^{17} 1 MeV n_{eq}/cm^2, the design of radiation-resistant particle detectors becomes of utmost importance. To this purpose, Technology Computer-Aided Design (TCAD) simulations are a relevant part of the current detector R&D, not only to support the sensor design and optimization, but also for a better understanding and modelling of radiation damage. In this contribution, the recent advances in the TCAD modelling of non-irradiated and irradiated LGAD sensors are presented, whose validation relies on the agreement between the simulated and experimental data — in terms of current-voltage (I-V), capacitance-voltage (C-V), and gain-voltage (G-V) characteristics, coming from devices manufactured by Hamamatsu Photonics (HPK), and accounting for different irradiation levels and temperatures.

Keywords: Detector modelling and simulations I (interaction of radiation with matter, interaction of photons with matter, interaction of hadrons with matter, etc); Detector modelling and simulations II (electric fields, charge transport, multiplication and induction, pulse formation, electron emission, etc); Radiation-hard detectors; Solid state detectors

*Corresponding author.

https://doi.org/10.1088/1748-0221/19/01/C01022

2024 JINST 19 C01022

Contents

1 Introduction

In recent years, the Low-Gain Avalanche Diode (LGAD) technology [1] has gained growing interest within the high-energy physics (HEP) community as detectors of choice for high precision tracking in space and time [2]. For example, they have been selected to operate in the Endcap Timing Layer (ETL) of the CMS experiment [3] and in the High-Granularity Timing Detector (HGTD) of the ATLAS experiment [4] for the forthcoming High-Luminosity phase of the Large Hadron Collider (HL-LHC) at CERN. In this scenario, the maximum fluence foreseen will exceed $1 \times 10^{16}\,\mathrm{cm}^{-2}$ 1 MeV equivalent neutrons ($\mathrm{n_{eq}}$), whereas in the next generation of high-energy and high-intensity hadron colliders (e.g., the hadronic Future Circular Collider [5]) the fluences will be even higher by more than an order of magnitude, up to about $5 \times 10^{17}\,\mathrm{n_{eq}/cm^2}$.

The behaviour of silicon sensors under extreme irradiation needs to be investigated and properly modelled to understand the complex physical phenomena related to radiation damage effects, and to design tracking detectors that efficiently work at that unprecedented radiation levels. To this purpose, modern Technology Computer-Aided Design (TCAD) tools allow to model and predict in advance the electrical behaviour of solid-state devices in different operating conditions, by suitably balancing physical accuracy, application versatility and computational demand.

In this work, the state-of-the-art Synopsys Sentaurus TCAD [6] suite of tools was used to validate a recently developed numerical model for the simulation and design of LGAD sensors [7]. The comparison between simulation findings and experimental data, which were obtained by measuring in different operating conditions (i.e., bias, fluence and temperature) two different types of LGAD sensors coming from the second production run of Hamamatsu Photonics (HPK), as well as the detailed description of the TCAD model and the adopted experimental techniques are presented and discussed.

2 Experimental techniques for the characterization of LGAD sensors

This paragraph describes the experimental techniques used for the characterization of the LGAD sensors considered for this work. In the following, the tested samples and the employed measurement setups and methods are described (section 2.1), as well as the experimental data obtained from the measurements of samples before and after irradiation are presented (section 2.2).

2024 JINST 19 C01022

2.1 Devices under test, experimental setups and methods

The Devices Under Test (DUT) considered for this study were LGAD sensors coming from the second production run of HPK, called HPK prototype 2 (HPK2). They are characterized by a 50 µm-thick high-resistivity epitaxial layer, and by a deep and narrow Gain Layer (GL) doping profile which was designed and produced in four different splits (S1-S4) that differ in the doping concentration. The measurements reported in section 2.2 refer to the first two splits, namely S1 and S2, which were conceived for the R&D of the timing detectors in the ATLAS experiment. The samples have an active area of $1.3 \times 1.3\,\mathrm{mm}^2$ and a Guard Ring (GR) structure surrounding the central pad. In table 1 the main parameters of the samples before irradiation are listed. The GL depletion voltage (V_{GL}), the breakdown voltage (V_{BD}) measured at room temperature (RT), and the capacitance reached above full depletion (C_{FD}) are given.

The electrical characterization in absence of external stimulus was performed both at the "Laboratory for Innovative Silicon Sensors" (LISS) of the INFN Torino Unit, and at the clean room of the INFN Perugia Unit. A temperature-controlled probe station electrically connected to a device analyzer was used to extract the key physical quantities, such as the current-voltage (I-V) and capacitance-voltage (C-V) characteristics. The samples were placed and kept by a vacuum system directly on a chuck, which provided the high reverse voltage (i.e., a negative voltage for the n-in-p LGAD sensors studied in this work). During the electrical characterization the GR was connected to the ground, and a high-current resolution Medium Power Source and Monitor Unit (MP-SMU) or a Multi-Frequency Capacitance Measurement Unit (MF-CMU) were connected to the pad under test dependently on the chosen measurement (I-V or C-V, respectively). More details about the I-V and C-V setups can be found in [8].

The gain of the LGAD samples before and after irradiation was measured at LISS. It was evaluated as the ratio between the charge measured in the LGAD and the expected charge from a 50 µm-thick p-i-n diode after its full depletion (i.e., 0.5 fC). Regarding the gain measurements of non-irradiated samples, a pulsed (1 kHz) infrared (IR)-laser with a wavelength of 1060 nm in the Top Transient Current Technique (Top-TCT) setup was used. The IR-laser intensity was tuned to generate an equivalent charge of about 3 Minimum Ionizing Particles (MIP) in the detectors and the spot size was of about 10 µm. The gain of the irradiated LGAD samples, instead, was measured by using a temperature-controlled β-source setup. A two-planes setup configuration (i.e., DUT and time reference, the latter used also as a trigger) was used to ensure that the β-particles (i.e., the electrons emitted by a ^{90}Sr source) are MIP equivalent. A dedicated read-out board with current-mode high-bandwidth amplifiers was used to readout both the DUT and the time reference signals. More details about the used TCT and β-source setups can be found in [8].

Table 1. Measured parameters of the LGAD samples used in this work before irradiation. The GL depletion voltage (V_{GL}), the breakdown voltage (V_{BD}) at room temperature (RT), and the capacitance reached above full depletion (C_{FD}) are given.

Sample	V_{GL} [V]	V_{BD} (RT) [V]	C_{FD} [pF]
$S1$	54.5	152	3.7
$S2$	53.5	172	3.8

2024 JINST 19 C01022

2.2 Measurements before and after irradiation

The C-V measurements of the non-irradiated samples were performed at RT, and the frequency of the sinusoidal signal delivered by the device analyzer was set to 100 kHz with an amplitude of 0.5 V. Figure 1(a) and figure 1(b) show the C-V and $1/C^2$-V curves of the two different LGAD samples before irradiation. Such curves allowed for identifying the V_{GL} and C_{FD} values reported in table 1, as well as the extraction of the GL implant profiles (i.e., amplitude, width and depth from the junction) given in figure 1(c). In particular, the depth d and the active doping concentration N_A as a function of the depth d were computed by using the following equations:

$$d = \frac{\epsilon_{Si} A}{C}, \qquad N_A = \frac{2}{\epsilon_{Si} q A^2 \frac{\partial 1/C^2}{\partial V}}. \tag{2.1}$$

where ϵ_{Si} is the silicon dielectric constant, A is the active area of the sensor, and q is the elementary charge. The C-V measurements of the irradiated samples, instead, were performed at 298 K with a measurement frequency and amplitude of the sinusoidal signal of 2 kHz and 0.5 V, respectively. Figure 2(a) and figure 2(b) show the C-V and $1/C^2$-V curves of the two different LGAD samples after irradiation. It is evident the reduction of the V_{GL} and the increase of the voltage of full depletion (V_{FD}) when the fluence (Φ) increases. Since the HPK2 production run was conceived for the R&D of the timing detectors of the ATLAS and CMS experiments, the sensors were irradiated up to the fluence of 2.5×10^{15} n_{eq}/cm^2, which is of interest for these two experiments. Therefore, all measurements shown in this work are performed up to this fluence value.

The I-V measurements of the non-irradiated and irradiated samples were performed at RT and 248 K, respectively. These are shown in figure 3(a). The curves of the non-irradiated samples allowed for identifying the V_{BD} values reported in table 1, as well as the gain of the two splits. In particular, the different exponential growth of their leakage current (I_{leak}) suggests that the gain of S1 is higher than the gain of S2 when the bias voltage is fixed. This is the direct consequence of the difference between the doping concentrations in the GL region of the two splits, as given in figure 1(c). The curves related to the irradiated samples, instead, show the expected increase of the I_{leak} and V_{BD} when Φ increases.

The gain of the non-irradiated samples was measured at RT by using the Top-TCT setup, whereas the gain of the irradiated ones was measured at 248 K by using the β-source setup. Figure 3(b) shows the gain-voltage (G-V) curves of the two different LGAD samples before and after irradiation. Before irradiation, the gain of S1 is higher than the gain of S2, as already observed in the I-V curves given in figure 3(a). The gain of the irradiated samples, instead, is almost the same when the bias voltage is fixed and, as expected, it decreases when Φ increases.

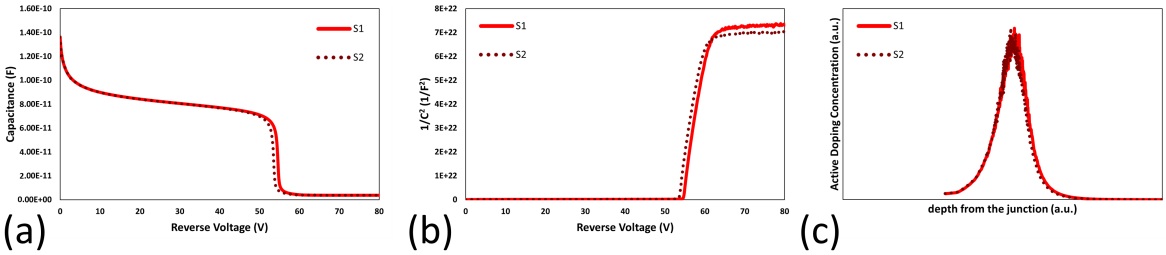

Figure 1. (a) C-V and (b) $1/C^2$-V characteristic curves of the two LGAD types used for this work, before irradiation. They were obtained at RT with a measurement frequency of 100 kHz. (c) GL doping profiles extracted from the C-V and $1/C^2$-V measurements by employing (2.1).

2024 JINST 19 C01022

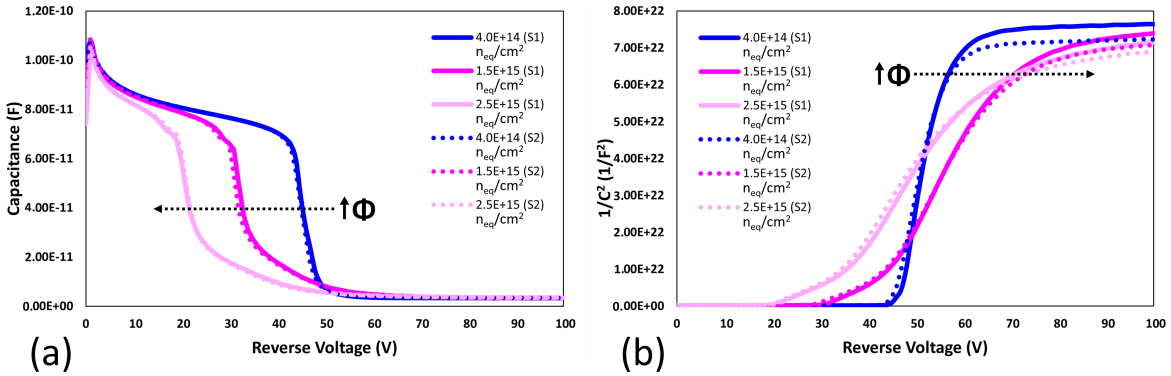

Figure 2. (a) C-V and (b) $1/C^2$-V characteristic curves of the two LGAD types used for this work, after irradiation. They were obtained at 298 K with a measurement frequency of 2 kHz.

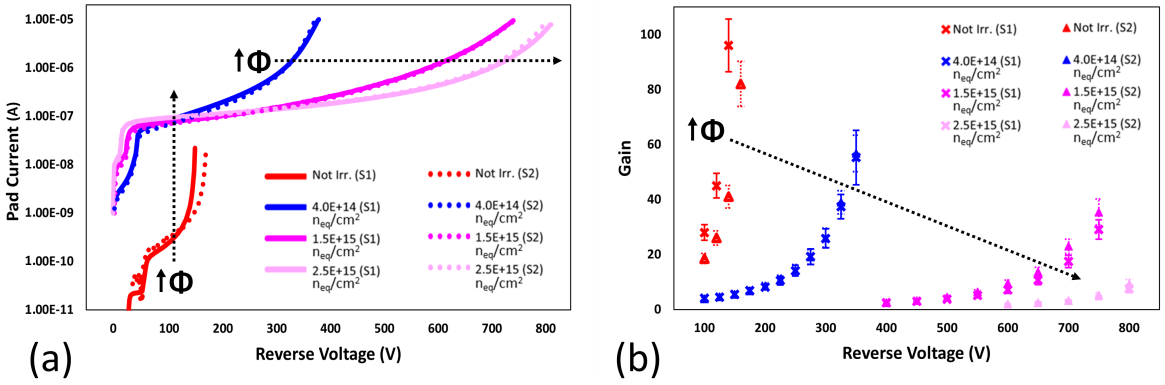

Figure 3. (a) I-V and (b) G-V characteristic curves of the two LGAD types used for this work, before and after irradiation. The characteristics before irradiation were obtained at RT, whereas the one after irradiation at 248 K. In particular, the G-V curves of the non-irradiated LGADs were obtained by using the scanning TCT-system, whereas the one of the irradiated samples were obtained by using the β-source setup.

3 TCAD model for the numerical simulation of LGAD sensors

This paragraph describes the TCAD model used for the numerical simulation of the LGAD sensors considered for this work. In particular, the layout and the doping profiles, as well as the radiation damage model employed for the simulations of the irradiated devices are described in section 3.1; the simulation findings and their comparison with the experimental data are presented in section 3.2.

3.1 Layout, doping profile and radiation damage model

The layout of the LGAD device was implemented within the TCAD by using the simple quasi-1D geometry depicted in figure 4(a). The periphery structures (i.e., the JTE and GR) were neglected because the simulations showed no significant differences when considering them or not.

The sensor active thickness, the bulk doping concentration and the GL doping profiles of S1 and S2 were extracted from the C-V and $1/C^2$-V measurements presented in section 2.2 and fed into the TCAD simulations. The measured V_{GL} and C_{FD} values were then used to fine-tune the GL implant profile. In particular, a slight shift of its position, and small variations in the sensor thickness and

2024 JINST 19 C01022

bulk doping concentration resulted in the perfect agreement between the measured and simulated C-V and $1/C^2$-V curves, as displayed in figure 5(a) and figure 5(b).

The radiation damage effects were modelled by means of the "Perugia Modified Doping" (PerugiaModDoping) TCAD radiation damage model, which was already validated by comparing simulations and measurements of sensors coming from the UFSD2 and UFSD3.2 production runs of Fondazione Bruno Kessler (FBK) [7]. Such model combines the traps parameterization of the "New University of Perugia" radiation damage model [9] with the fluence-dependent analytical parameterizations of the GL and bulk effective doping, called "Torino analytical parameterizations" [8]. Figure 4(b) shows the effect of such parameterizations on the effective doping, thanks to which it is possible to take into account in the TCAD simulations both the acceptor-removal mechanism in the GL [10] and the saturation of the acceptor-creation mechanism in the bulk [11].

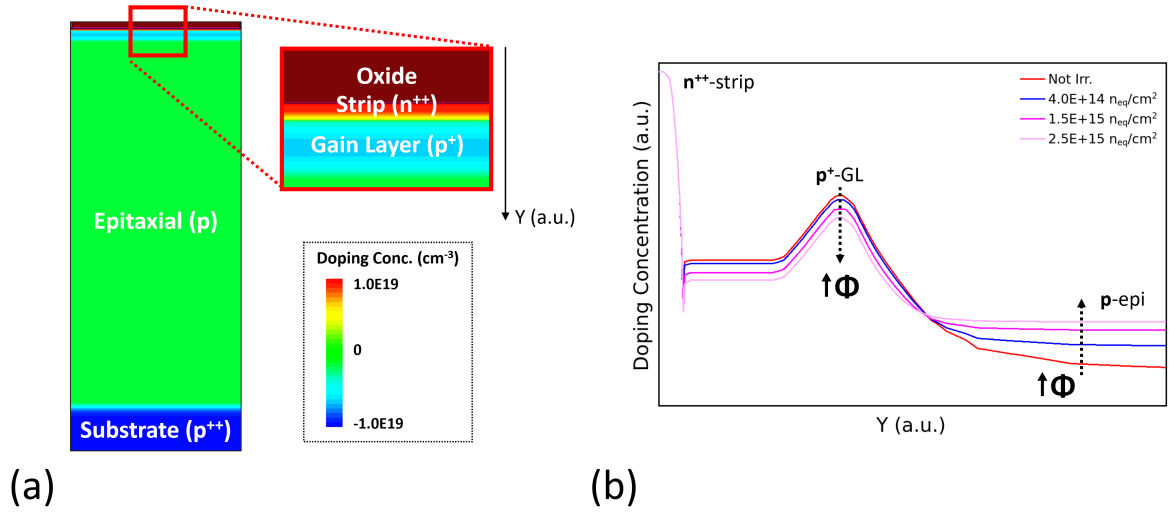

Figure 4. (a) Layout of the LGAD device implemented within the TCAD and (b) fluence-dependent evolution of the GL and bulk doping profiles according to the analytical parameterizations of the "PerugiaModDoping" radiation damage model. Gaussian profiles were used to model the highly doped n-type an p-type implants.

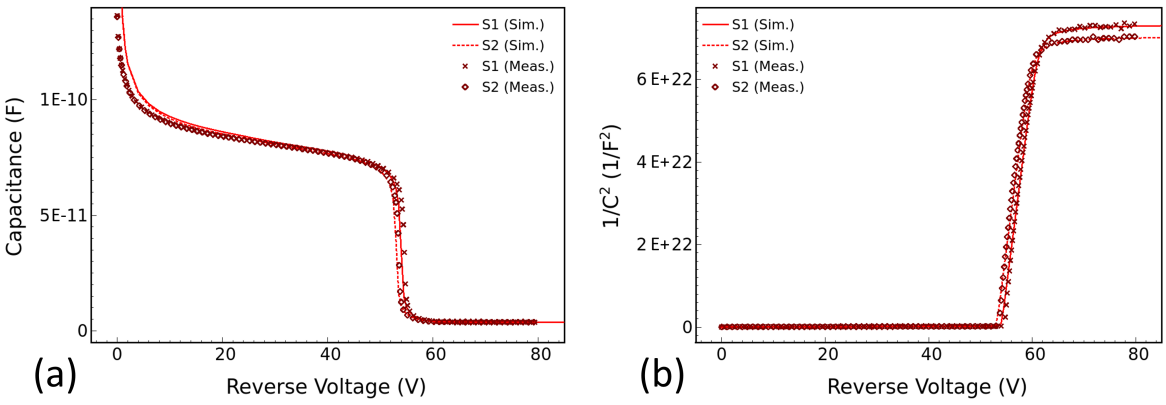

Figure 5. (a) C-V and (b) $1/C^2$-V simulated (solid lines) and experimental (markers) curves of the two LGAD types, carried out at 290 K with a frequency of 100 kHz to have a direct comparison with experimental data.

2024 JINST 19 C01022

3.2 Simulation findings and model validation

Once the model of the LGAD was implemented within the TCAD, the electrical behaviour and the response to an equivalent MIP stimulus under different operating conditions were simulated. To have a direct comparison with the experimental data, the simulations were performed in the same measurement conditions (i.e., temperature, frequency and irradiation level). Moreover, since the S1 and S2 behave at the same manner after irradiation as shown in section 2.2, all the comparisons between simulations and measurements after irradiation will refer only to one of the two splits in the following.

The C-V curves of the LGAD after irradiation were simulated at 298 K, and the frequency of the sinusoidal signal was set to 2 kHz with an amplitude of 0.5 V. In figure 6(a) and figure 6(b), the simulated C-V and $1/C^2$-V curves of S1 after irradiation are shown and compared with the measurements. The reduction of the V_{GL} and the increase of the V_{FD} when Φ increases were well reproduced in simulation.

The I-V curves of the non-irradiated LGAD were simulated at 290 K, instead the ones after irradiation were simulated at 248 K. Special attention were devoted to the choice of the avalanche model, by investigating among two different versions of the Van Overstraeten-De Man (vOv) model: the default TCAD-embedded one [12], and the one which uses a new set of parameters for the impact ionization coefficients [13]. Figure 7(a) gives a comparison of the experimental and simulated curves of S1 before and after irradiation. A good matching was obtained in terms of V_{BD} when using the default avalanche model before irradiation, and the new one after irradiation. No differences were observed by using the two versions of the avalanche model, instead, in terms of increase of I_{leak} when Φ increases.

By performing transient simulations of the passage of an equivalent MIP stimulus, the gain for a given voltage was obtained as the ratio between the charge collected in the LGAD and the charge collected in the corresponding p-i-n diode under the same operating conditions. In particular, the gain of the non-irradiated LGAD was simulated at 290 K, whereas the one of the LGAD after irradiation was simulated at 248 K. As shown in figure 7(b), a good agreement between the experimental and simulated curves was obtained before and after irradiation.

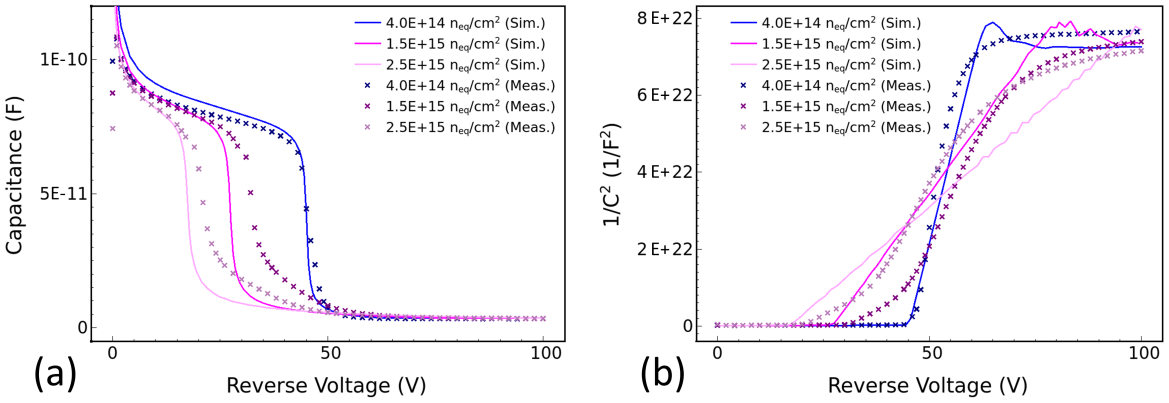

Figure 6. (a) C-V and (b) $1/C^2$-V simulated (solid lines) and experimental (markers) curves related to S1, carried out at 298 K with a frequency of 2 kHz, after irradiation.

2024 JINST 19 C01022

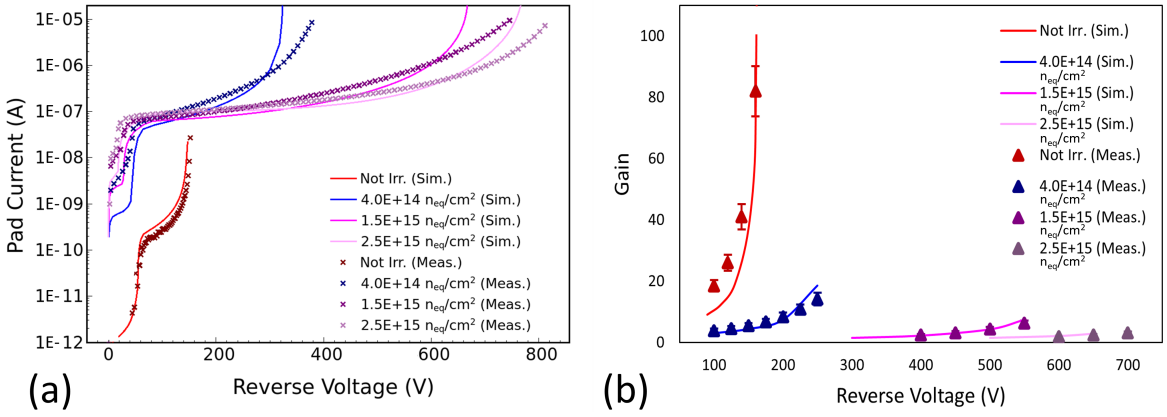

Figure 7. (a) I-V and (b) G-V simulated (solid lines) and experimental (markers) curves related to S1 and S2, respectively. The curves before irradiation were simulated at 290 K by using the vOv avalanche model [12], whereas the ones after irradiation were simulated at 248 K by using a new version of such model [13].

4 Conclusions

In this work, the validation of a TCAD model for the numerical simulation of LGAD sensors conceived for particle detection in the next generation of HEP experiments is presented. The model robustness and generality (e.g., in terms of operating conditions of the sensor, vendors and/or technology options) were evaluated with the aid of TCAD simulations based on a recently proposed model for the numerical simulation of radiation damage effects on LGAD sensors, called "PerugiaModDoping" [7]. To this end, extensive measurement campaigns were performed on two different splits of LGAD sensors coming from the second production run of Hamamatsu Photonics (HPK), in order to extrapolate the electrical characteristics (i.e., I-V, C-V and G-V curves), and the responses of the sensors to different stimuli (laser and β-particles source) under different operating conditions (i.e., temperature, frequency and irradiation level). The model validation relies on the comparison between simulation results and experimental data which were found to be in good agreement for all the tested devices and for all the considered irradiation fluences. This not only qualifies the suitability of the adopted model to accurately reproduce the electrical characteristics of LGAD sensors, but also enables the prediction of their performance and the advancement of new sensor technologies to be used in the future HL-LHC scenario.

Acknowledgments

This project has received funding from the European Union's Horizon 2020 research and innovation programme under GA No 101004761 and from the Italian MIUR PRIN under GA No 2017L2XKTJ. The work is performed in collaboration with the INFN CSN5 "eXFlu" research project.

References

[1] G. Pellegrini et al., *Technology developments and first measurements of Low Gain Avalanche Detectors (LGAD) for high energy physics applications*, *Nucl. Instrum. Meth. A* **765** (2014) 12.

[2] H.F.W. Sadrozinski, A. Seiden and N. Cartiglia, *4D tracking with ultra-fast silicon detectors*, *Rept. Prog. Phys.* **81** (2018) 026101 [arXiv:1704.08666].

2024 JINST 19 C01022

[3] CMS collaboration, *Technical proposal for a MIP timing detector in the CMS experiment Phase 2 upgrade*, CERN-LHCC-2017-027, LHCC-P-009 (2017) [DOI:10.17181/CERN.2RSJ.UE8W].

[4] ATLAS collaboration, *Technical Proposal: A High-Granularity Timing Detector for the ATLAS Phase-II Upgrade*, CERN-LHCC-2018-023, LHCC-P-012 (2018) [DOI:10.17181/CERN.CIUJ.KS4H].

[5] FCC collaboration, *FCC-hh: The Hadron Collider: Future Circular Collider Conceptual Design Report Volume 3*, *Eur. Phys. J. ST* **228** (2019) 755.

[6] Synopsys Sentaurus TCAD (Online), available: https://synopsys.com/.

[7] P. Asenov et al., *TCAD modeling of bulk radiation damage effects in silicon devices with the Perugia radiation damage model*, *Nucl. Instrum. Meth. A* **1040** (2022) 167180.

[8] M. Ferrero et al., *An Introduction to Ultra-Fast Silicon Detectors*, 1st edition, CRC Press (2021) [DOI:10.1201/9781003131946].

[9] A. Morozzi, F. Moscatelli, D. Passeri and G.M. Bilei, *TCAD advanced radiation damage modeling in silicon detectors*, *PoS* **Vertex2019** (2020) 050.

[10] M. Moll, *Acceptor removal — Displacement damage effects involving the shallow acceptor doping of p-type silicon devices*, *PoS* **Vertex2019** (2020) 027.

[11] V. Sola et al., *Next-generation tracking system for future hadron colliders*, *PoS* **Vertex2019** (2020) 034.

[12] R. Van Overstraeten and H. De Man, *Measurement of the ionization rates in diffused silicon p-n junctions*, *Solid-State Electron.* **13** (1970) 583.

[13] E. Curras Rivera and M. Moll, *Study of Impact Ionization Coefficients in Silicon With Low Gain Avalanche Diodes*, *IEEE Trans. Electron. Dev.* **70** (2023) 2919 [arXiv:2211.16543].

2024 JINST 19 C01022